V4 Japan project

Report 10-07-2017

by Aleš Jäger, Karel Tesař, Jiří Němeček

1. Samples

AZ31 magnesium alloy (nominally Mg-3Al-1Zn-0.2Mn in wt%) in the form of microtubes received from AGH on April 2017 were analysed. The specimens were characterised with various techniques including atomic force microscopy (AFM), light microscopy (LM), 3D light microscopy (3D LM), scanning electron microscopy (SEM) and energy dispersive spectroscopy (EDS) attached to SEM.

1.1 Labelling, dimensions and surfaces

For the sake of clarity, the samples are shown in Fig.1. Four different processing states and surface treatments of AZ31 microtubes were analysed. The samples are labelled A1, A2, B1 and B2. A1 and B1 are samples after laser dieless drawing techniques, which are without and with graphite painting, respectively. A2 and B2 are as-extruded AZ31 tubes without and with graphite painting, respectively. The purpose of graphite painting is to enhance thermal exchange between laser beam and AZ31 surface during dieless drawing. The as-extruded samples introduced "precursor" for subsequent laser dieless drawing. An average dimensions (inner diameter/wall thickness) of the microtubes A1, B1, A2 and B2 were 2.16 mm/0.71 mm, 3.16 mm/ 0.35 mm, 3.10 mm/ 0.82 mm and 4.24 mm/ 0.48 mm, respectively.

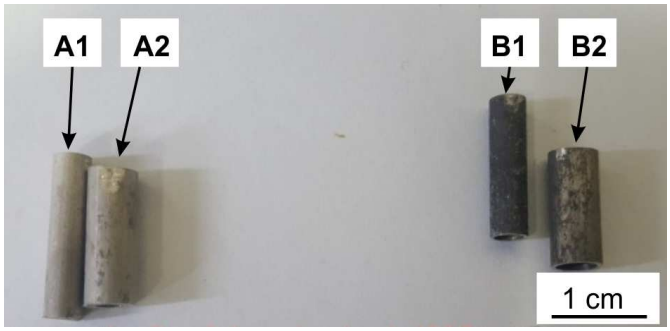

Fig. 1: Four different samples of the AZ31 microtubes with labelling.

2. Microstructural analysis

This part summarizes analysis of microstructural features via LM (Zeiss Axio Observer D1m). Grain size, grain shapes, grain size gradients, impurities, inclusions and phases were analysed.

2.1 Sample preparation

Microstructures of both the **longitudinal (AD-RD plane)** and **transversal (RD-RD plane)** planes were analysed for each sample in Fig. 1. The planes are schematically depicted in Fig. 2. AD and RD stands for axial and radial direction, respectively. For longitudinal plane analysis, the samples were cut longitudinally into two halves. The samples were then mechanically grinded using a SiC paper with P2000 grit. Thereafter, 3 µm and 1 µm polycrystalline diamond suspensions were used for delicate mechanical polishing. As the last step, a mechanical-chemical polishing using Struers OP-S solution was applied. The polished surfaces were afterwards etched using 8 vol.% water solution of HNO_3 in order to reveal grain boundaries.

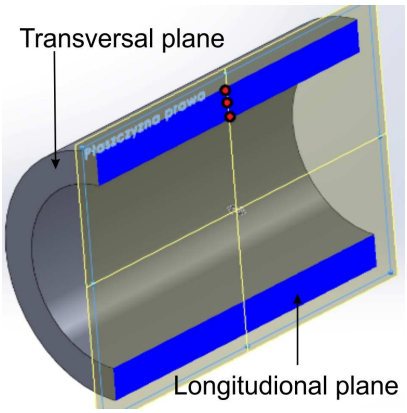

Fig. 2: Scheme of the planes used for LM analysis

For each plane (AD-RD and RD-RD) of each sample a minimum of 10 LM images were obtained at all available magnifications. From these images, a total of 4 images for each sample were chosen which provided the best possible detail for subsequent tube dimension analysis. The analysis itself consisted of fitting an inner circle and two circle segments for the determination of RD-RD dimensions, namely the tube diameter and thickness. AD-RD tube dimensions were determined in a same manner with the use of two parallel lines. In case of precise fitting, for instance with the least-square method, the standard deviation would be given. In case of these images, and for the required precision, the fitting of geometrical shapes was done by using naked eye and Corel Suite software. This approach was determined to be effective. Therefore, there is no standard deviation given for values shown in the images. Since the inner diameter inconsistency (AD-RD plane) can arise due to imprecise cutting in the centre of the tube, only standard deviation values of the tube thickness are presented and considered.

2.2 Light microscopy results

2.2.1 Tube dimensions

A1 – laser dieless drawing (not painted)

RD-RD plane

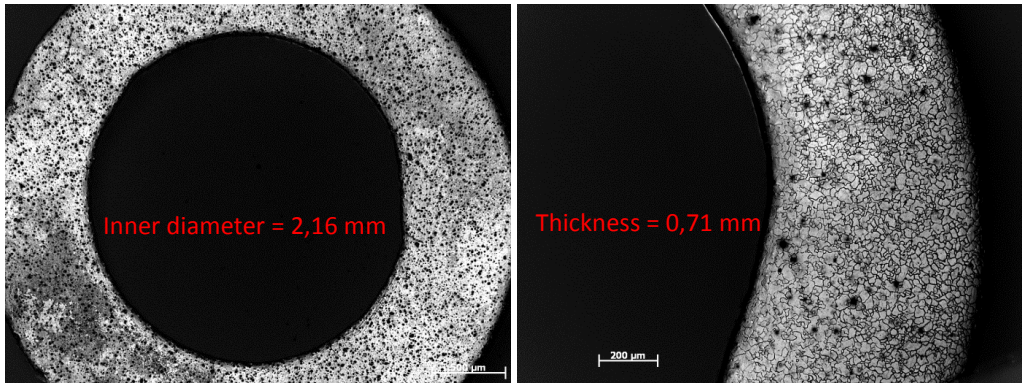

AD-RD plane (inner diameter calculated as an average of the maximal and minimal value)

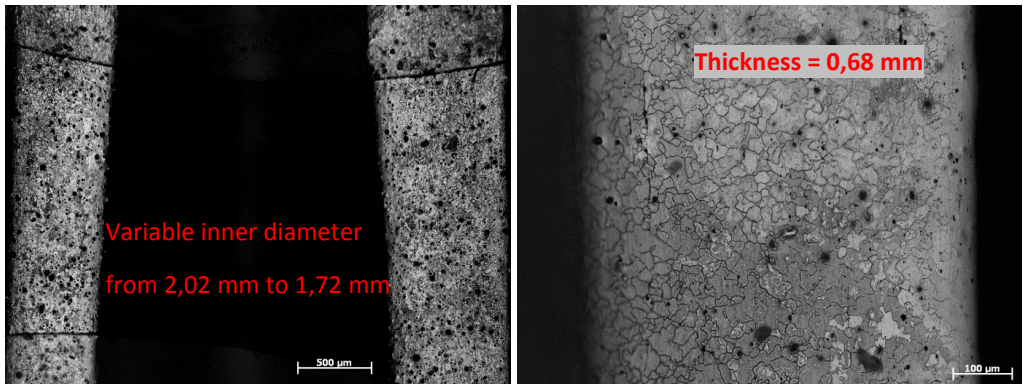

A1 Average inner diameter = **2.16 mm**

A1 Average tube thickness = (**0.69±0.02) mm**

A2 – as-extruded (not painted)

RD-RD plane

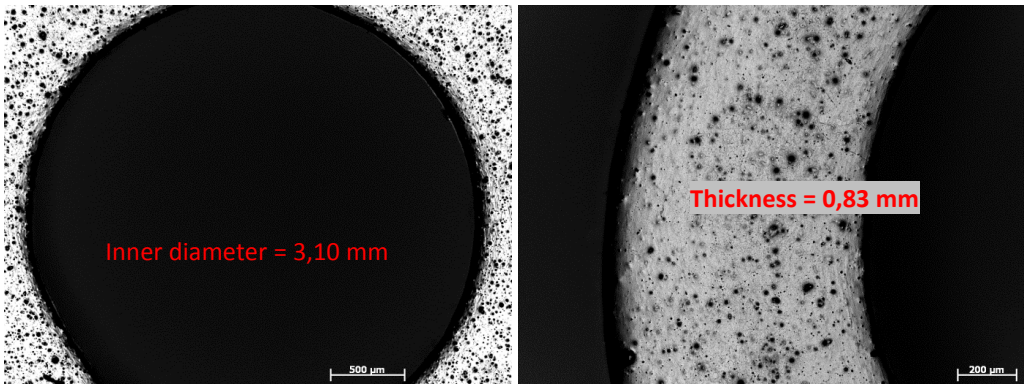

AD-RD plane

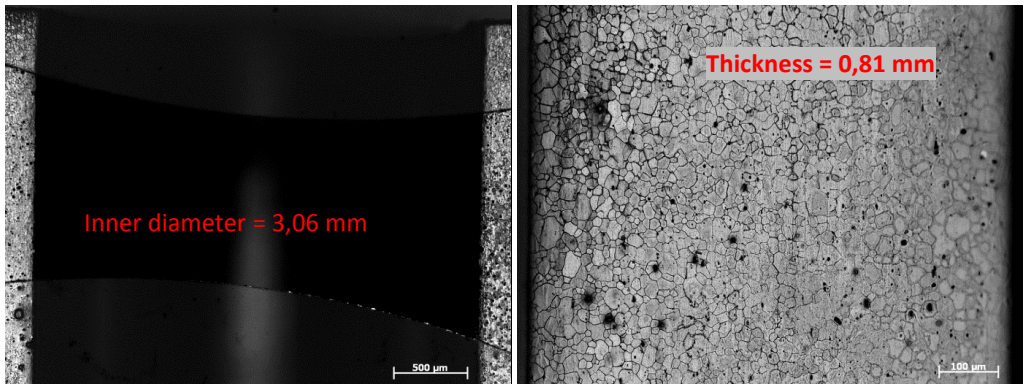

A2 Average inner diameter = **3.10 mm**

A2 Average tube thickness = (**0.82±0.01) mm**

B1 – laser dieless drawing (graphite painted)

RD-RD plane

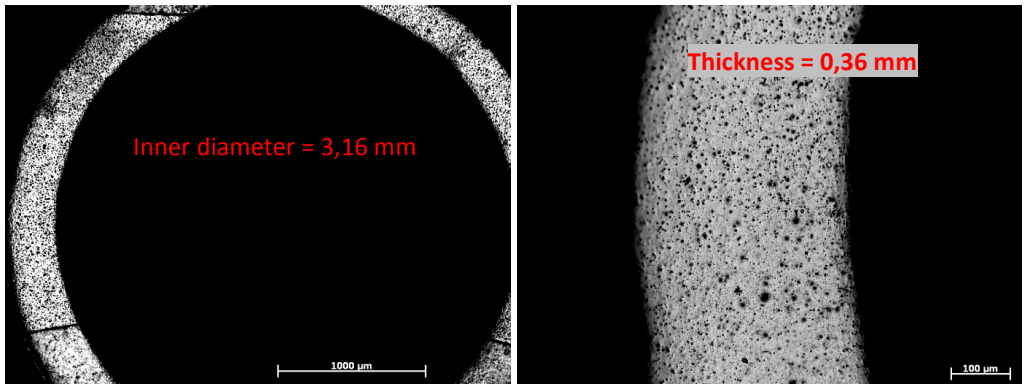

AD-RD plane

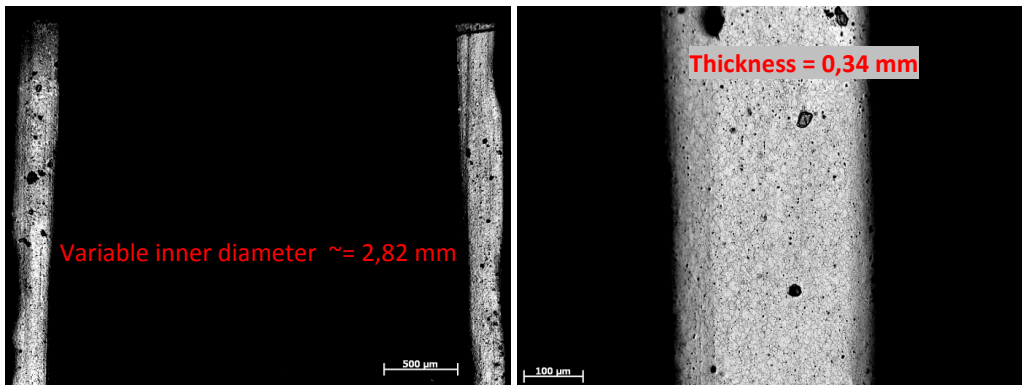

B1 Average inner diameter = **3.16 mm**

B1 Average tube thickness = (**0.35±0.01) mm**

B2 – as-extruded (graphite painted)

For the sample B2 tube dimensions were too large to measure them using the same approach as before. Only one value is considered.

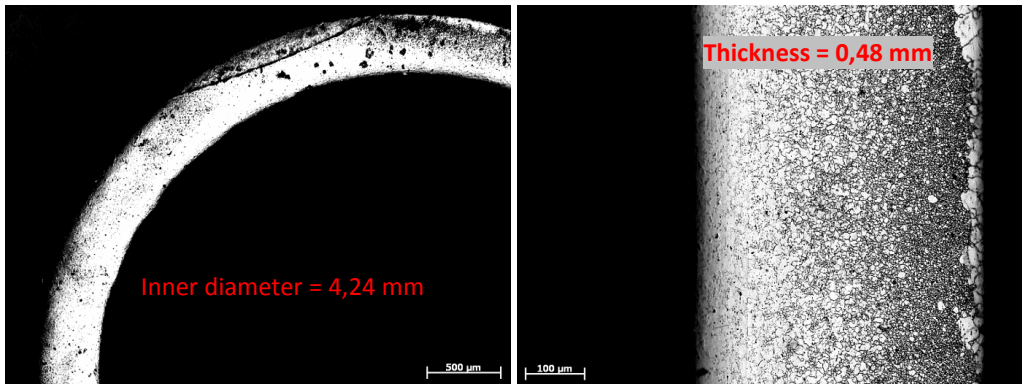

B2 Average inner diameter = **4.24 mm**

B2 Average tube thickness = **0.48 mm**

Fig. 3: LM of etched surfaces at low magnifications showing microtubes dimensions.

2.2.2 Grain size measurements

For grain size evaluation, the LM images with higher magnification than those in chap. 2.2.1 were used. Two the most typical micrographs were chosen for each sample (one in RD-RD and one in AD-RD plane). These micrographs were thereafter analysed using the Linear Intercept Method (LIN), with five horizontal and five vertical lines across each micrograph. An example of grain size evaluation is shown in Fig. 3.1. Resulting mean

intercept length was multiplied by geometrical factor of 1.74 to obtain an average grain size. This factor is a result of stereographical calculations determined in the literature [*see B Roebuck, C Phatak and I Birks-Agnew, A Comparison of the Linear Intercept and Equivalent Circle Methods for Grain Size Measurement in WC/Co Hardmetals, NPL Report MATC(A)149, National Physical Laboratory Teddington, Middlesex TW11 0LW, UK (2004)*].

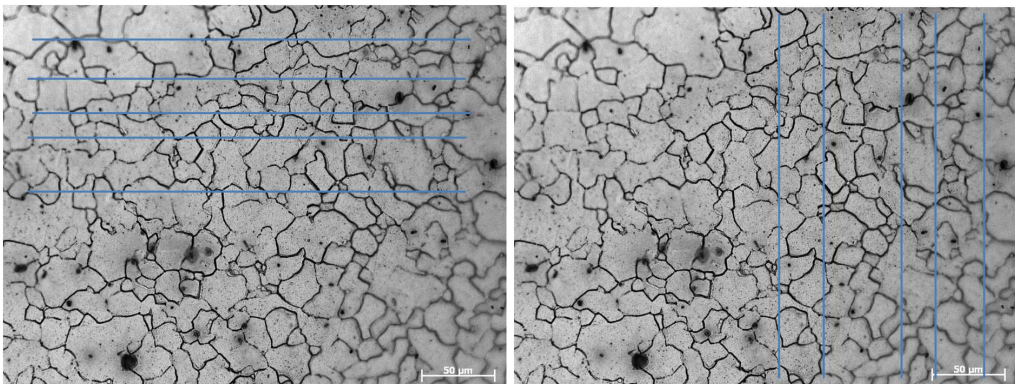

Fig. 4: Example of five horizontal and five vertical analyzed lines (A1 sample). Scale bar shows 50 μm.

For each sample and each plane we provide bellow three micrographs, **of which the most left one was analysed for grain size**. This method is not suitable to provide reasonable standard deviation value as the normal distribution of grain size cannot be expected. The standard deviation of grain size is normally provided only when the analysis is carried out by a more advanced technique which is able to determine complete grain size distribution histogram, like electron backscatter diffraction (EBSD). This is not necessary for this microstructure and required precision.

Typical microstructures of all samples are shown in Fig. 5. As can be seen, the grains are reasonably equiaxed for all samples despite intensive forming. This is a consequence of processing well above recrystallization temperature for both extrusion and laser dieless drawing. It has been shown by many authors that the recrystallization in moderately deformed AZ31 alloy takes place above 200°C and accelerates with increasing temperature. For example, the temperature measured in the deformation zone during stationary phase of the laser dieless drawing process is ~400 °C. Similar temperatures had to be used for extrusion. The grain size is practically the same for both forming techniques.

Besides impurities, in some LM images can also be seen second phase particles. Although EDS of the polished surface was not performed, the typical phases which can be found in AZ31 alloy are Mn based. Mn is added in small quantities to the AZ series of magnesium alloys to attract heavy impurities (e.g. Fe) and thus improve corrosion properties. However, Al and Zn based phases cannot be excluded as well (especially Mn-Al) despite both elements are under solubility limit in magnesium to facilitate forming. AZ31 is the most common Mg alloy for forming processes and it is well known that presence of hard yet brittle intermetallic phases hinder forming.

Numerical results extracted from the images in Fig. 5 are summarized in the Table 1.

A1 (RD-RD)

x average Grain size = 27.8 um; y average Grain size = 22.3 um; average RD Grain size = 25.1 um

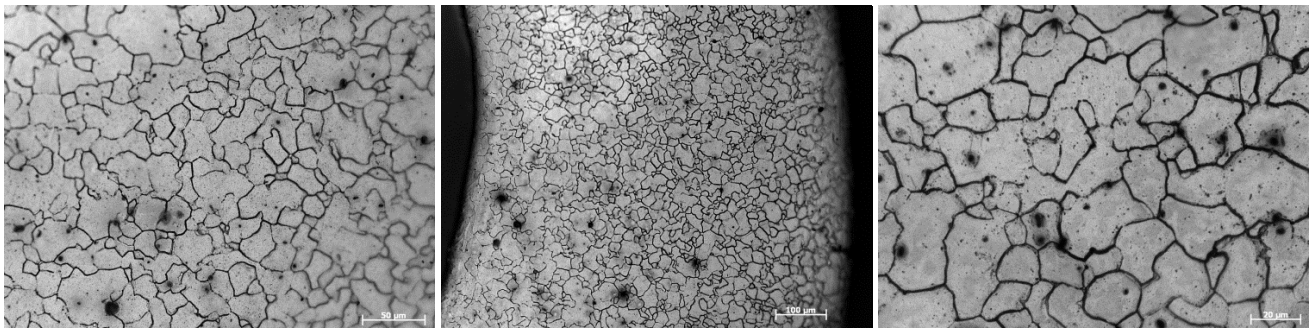

A1 (AD-RD)

RD average Grain size = 32.2 um; AD average Grain size = 24.5 um

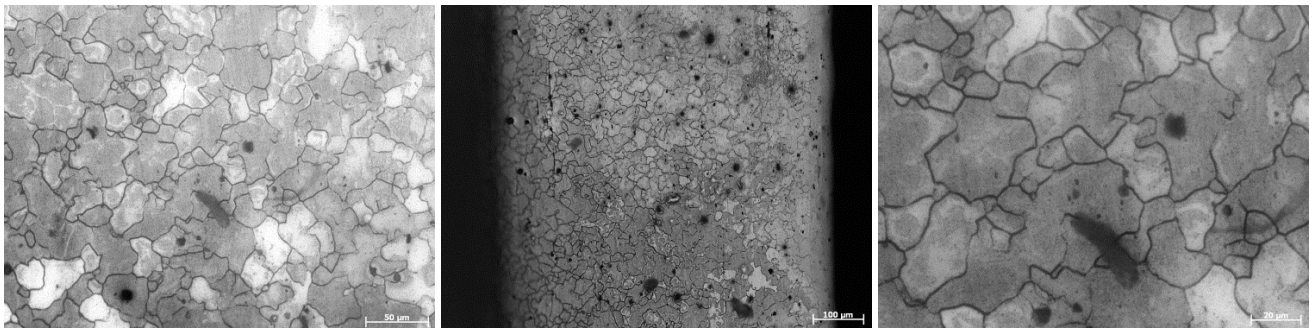

A2 (RD-RD)

x average Grain size = 23.3 um; y average Grain size = 25.3 um; average RD Grain size = 24.3 um

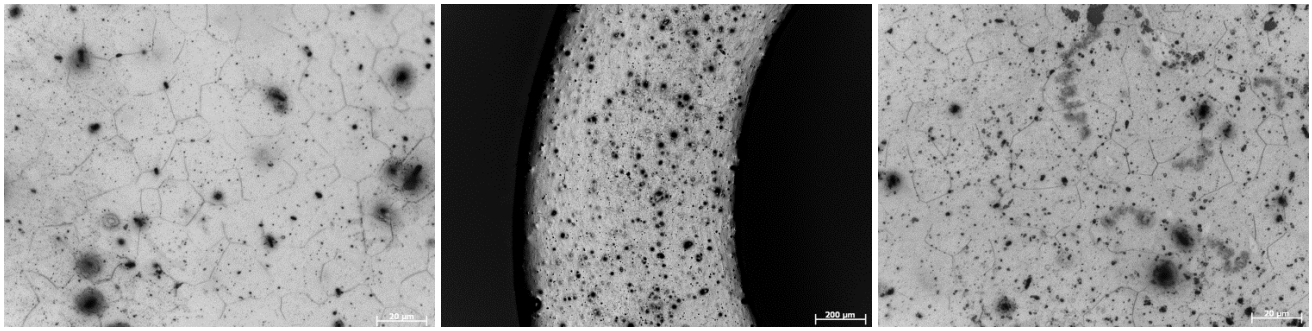

A2 (AD-RD)

RD average Grain size = 22.9 um; AD average Grain size = 20.2 um

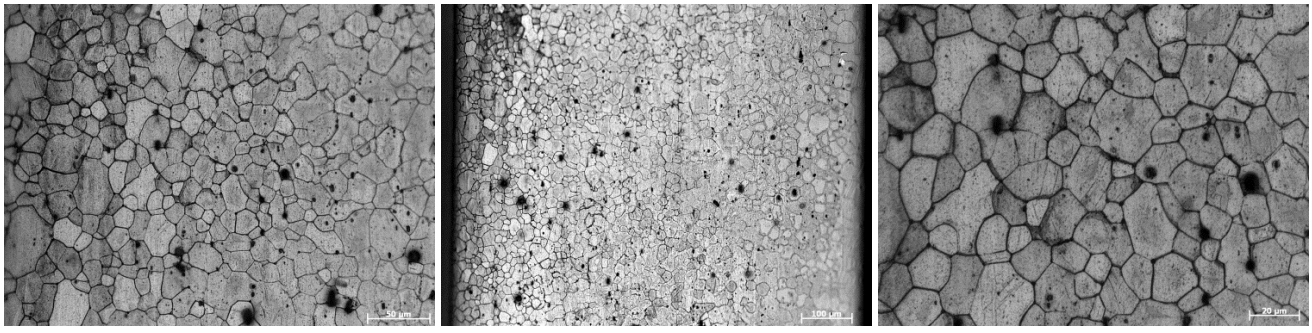

B1 (RD-RD)

x average Grain size = 7.6 um; y average Grain size = 8.6 um; average RD Grain size = 8.1 um

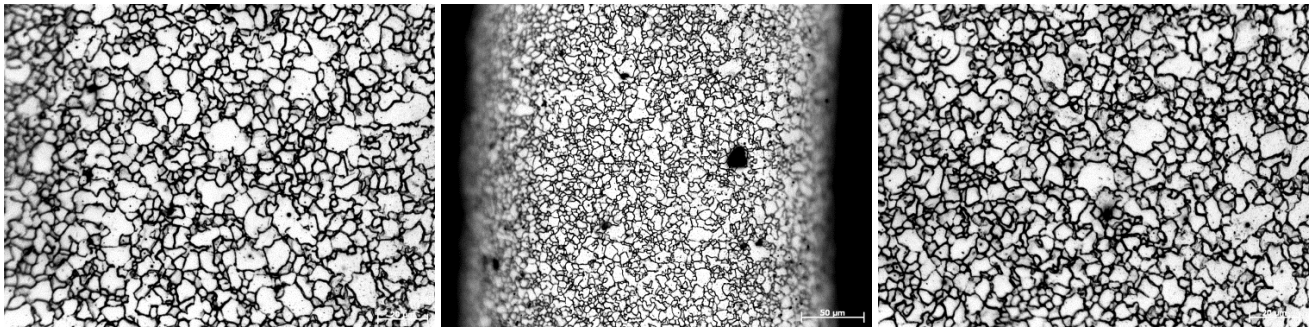

B1 (AD-RD)

RD average Grain size = 7.6 um; AD average Grain size = 9.5 um

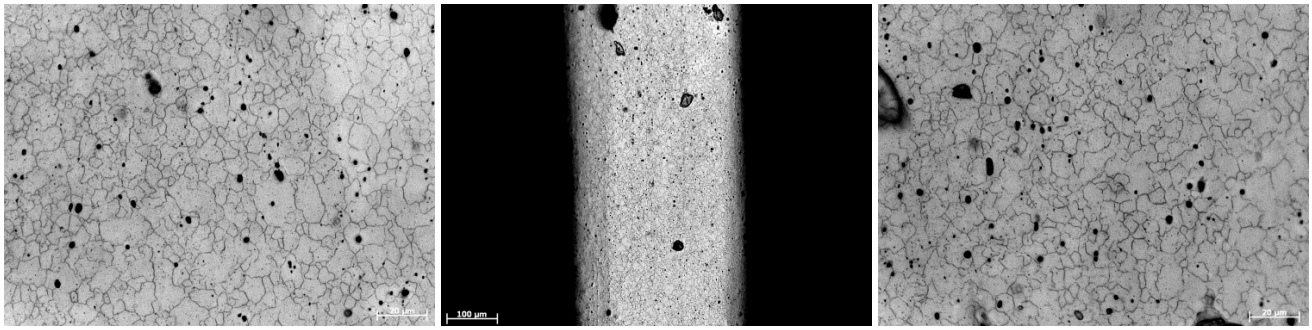

B2 (RD-RD)

x average Grain size = 7.6 um; y average Grain size = 8.3 um; average RD Grain size = 8.0 um

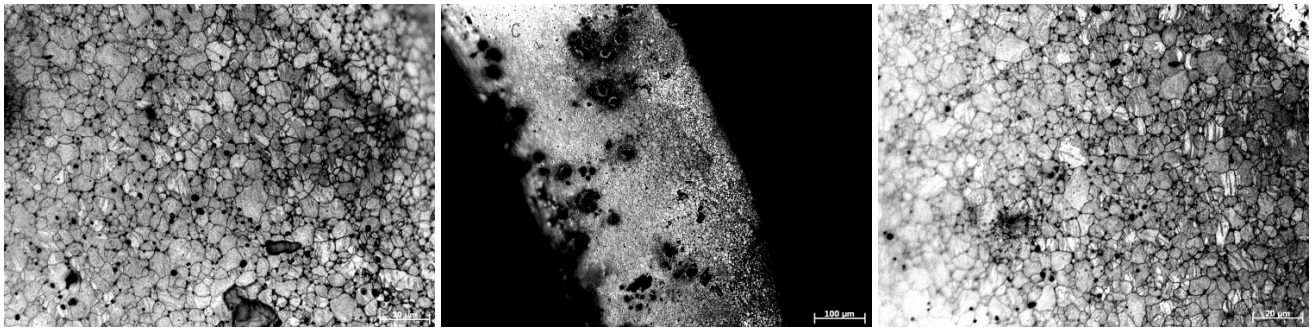

B2 (AD-RD)

High radial variations of grain size (constant in AD); Lower grain size near the outer surface (~3 um); Grain size on the inner side converges to the RD Grain size values

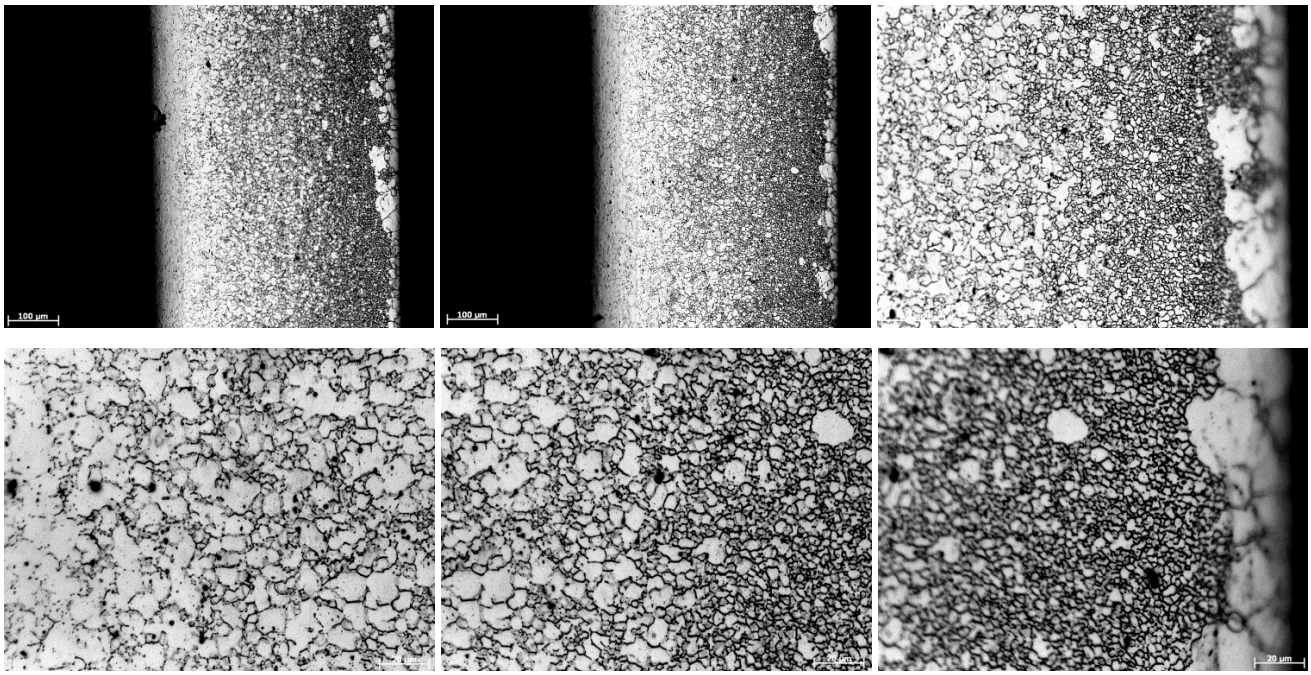

Fig. 5: Typical LM mirostructures of all samples at different magnifications and in different planes (etched surfaces)

Tab. 1: Numerical results extracted from LM for all samples. For plane description see chap. 2.1.

AD-RD plane (plane parallel to tube axis)				
Sample no.	**A1**	**A2**	**B1**	**B2**
x-line length (μm)	1500	1500	750	-
y-length length (μm)	1000	1000	652	-
RD intercept count	81	114	171	-
AD intercept count	71	86	114	-
RD average intercept (μm)	18.52	13.16	4.39	-
AD average intercept (μm)	14.08	11.63	5.48	-
Geometrical factor	1.74	1.74	1.74	-
RD average grain size (μm)	**32.2**	**22.9**	**7.6**	**-**
AD average grain size (μm)	**24.5**	**20.2**	**9.5**	**-**

RD-RD plane (plane perpendicular to tube axis)				
Sample no.	**A1**	**A2**	**B1**	**B2**
x-line length (μm)	1500	750	750	750
y-length length (μm)	1000	625	625	625
x intercept count	94	56	172	171
y intercept count	78	43	127	131
x average intercept (μ)	15.97	13.39	4.36	4.39
y average intercept (μm)	12.82	14.53	4.92	4.77
Geometrical factor	1.74	1.74	1.74	1.74
RD average grain size (μm)	**25.1**	**24.3**	**8.1**	**8.0**

A striking grain size inhomogeneity in radial direction was observed for B2 sample (Fig.6). Outer surface of the microtube showed a layer of large grains. However, the grain size in the middle and inner side converges to the RD-RD plane values of ~8 µm.

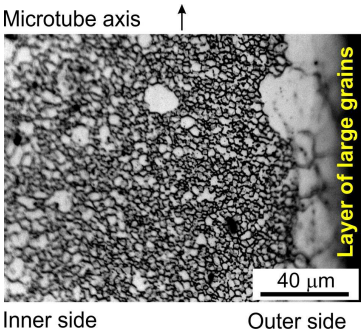

Fig. 6: Inhomogeneous grain size distribution in the sample B2.

2.3 SEM-EDS results

Fig. 7 shows chemical analysis of all microtube surfaces. If BSE image indicated several surface contracts, more than 1 site was analysed via EDS. Due to standardless method and limited resoution of the EDS, the precision is very limited especially for low concentrations and/or light elements (O and C). The elements detected were Mg, O, C, Al. Mg comes from the matrix, O is often present on metallic surfaces due to the oxidation and Al is the main alloying in the Mg matrix. Other elements (Si, Cl, Ca, Na) are uncertain and rather under resolution limit of the EDS. Although Zn is present in the matrix, it was not included in analysis by the mistake. However, its low concentration (~1wt.%) does not change quantification significatnly. Comparison of the results for various samples revealed some inconsistency because the samples A1 and A2 (without grafite paiting) show more carbon than the samples B1 and B2 (with grafite painting). Thus, the results must be viewed with some caution.

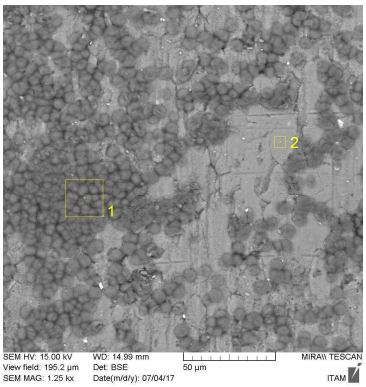

	1	*2*
Mg	30,56	77,75
O	52,13	8,49
C	16,1	11,31
Al	0,34	1,93
Si	0,16	
Cl	0,15	
Ca	0,21	
Na	0,37	0,52
total	100,02	100

Fig.7a: Chemical composition of the A1 surface (SEM-EDS) at sites 1 and 2.

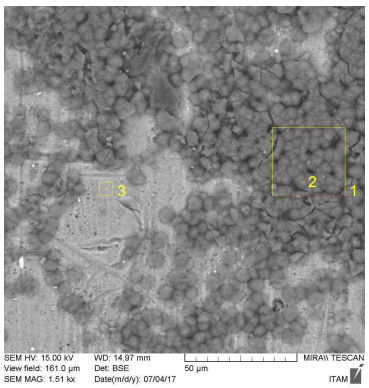

	1	*2*	*3*
Mg	25,2	59,33	84,55
O	54,72	23,28	4,17
C	19,52	16,99	8,97
Al	0,2	0,11	1,93
Si	0,14	0,08	
Na	0,23	0,21	0,37
total	100,01	100	99,99

Fig.7b: Chemical composition of the A2 surface (SEM-EDS) at sites 1, 2 and 3.

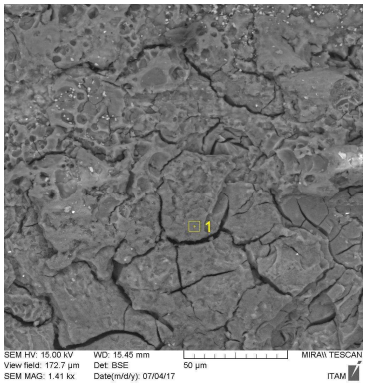

	1
Mg	34,53
O	55,65
C	7,93
Al	1,09
Si	0,25
Ca	0,27
Na	0,28
total	100

Fig.7c: Chemical composition of the B1 surface (SEM-EDS) at site 1.

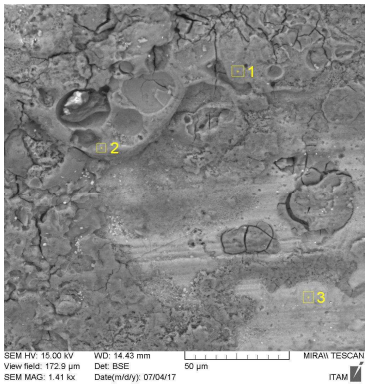

	1	*2*	*3*
Mg	39,65	33,35	86,92
O	50,89	57,41	11,39
C	6,65	9,24	1,4
Al	1,6		
Si	0,24		
Cl	0,49		
Ca	0,5		
Na			0,29
total	100,02	100	100

Fig.7d: Chemical composition of the B2 surface (SEM-EDS) at sites 1, 2 and 3.

3. Roughness analysis

3.1 Surface characterization via SEM

Several techniques listed in chapter 1 were employed to extract precise characteristics about surface roughness, morphology and chemical composition. Fig. 8 shows typical SEM micrographs of the surfaces at low (a) and high (b) magnification. It can be readily seen that significant differences in surface morphologies took place and various surface features were revealed. For SEM imaging, backscattered electron detector (BSED) was used because BSED is more sensitive to the atomic contrast than standard secondary electron detector. All surfaces indicate a presence of various corrosion products. The most probable chemistry of corrosion products is MgO and Mg(OH)2. Abundant surface oxide was confirmed with SEM-EDS. Significant part of the contrast in samples B1 and B2 is from graphite layer (Fig.8).

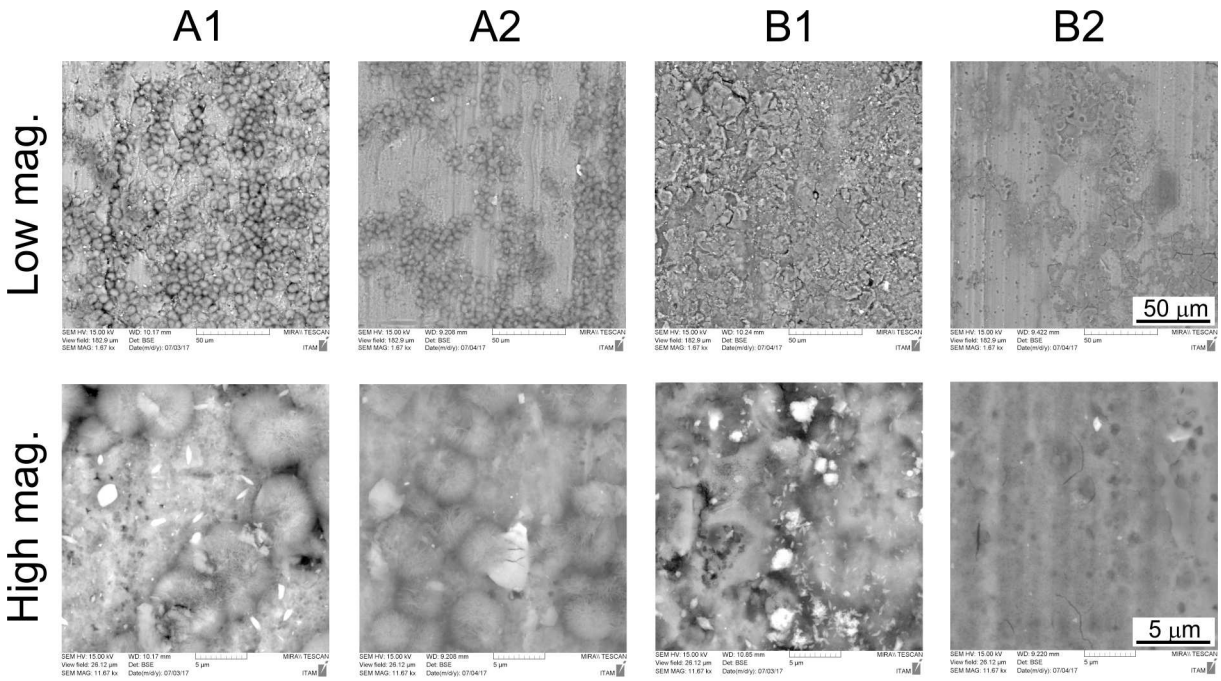

Fig. 8: Backscattered SEM images of the surfaces at two different magnifications (longitudinal axis of the microtubes is vertical).

3.2 Local roughness characterization via AFM

Fig. 9 shows typical examples of AFM maps for all samples at two different magnifications. Due to technical feasibility, only outer surfaces were observed via AFM. We can readily see notable differences in the surface morphologies of different samples as already indicated by SEM in Fig. 8. Numerical evaluation of the AFM maps with in-build software is shown in Tab.2. Several AFM maps for each sample were used to calculate an average surface roughness. This guarantee reasonable statistics and, thus reliable results. It is also worth noting that surface morphology often differs place to place.

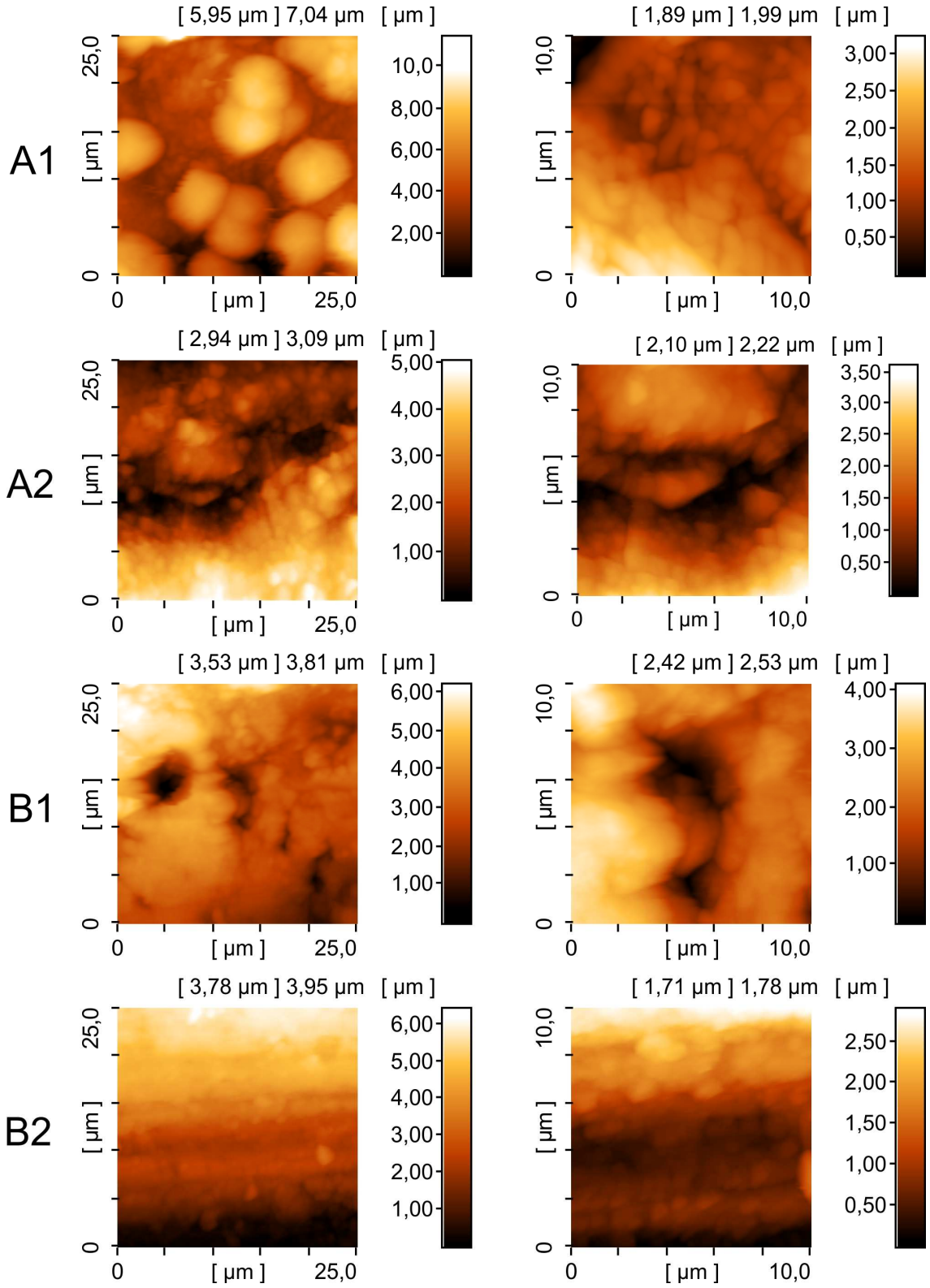

Fig. 9: Typical 3D surface morphology of all surfaces at two magnifications (AFM images, Longitudinal axis of the microtubes is horizontal).

Tab.2 lists the results of local roughness Rz (Ten-spot average roughness), Ry (Maximum height), Ra (average roughness) and Rq (root mean square roughness) of the surfaces as calculated from AFM measurements and evaluated via in-built software. We can see that local roughness parameters are very similar for all samples despite various surface morphologies shown in Figs. 8 and 9.

Tab.2: Local roughnesses Rz (Ten-spot average roughness), Ry (Maximum height), Ra (average roughness) and Rq (root mean square roughness) of the surfaces calculated from AFM measurements.

Sample no.	***A1***	***A2***	***B1***	***B2***
Average value of Rz (μm)	**5,5**	**5,1**	**5,7**	**4,3**
Standard deviation of Rz	1,5	1,9	2,0	1,3
Average value of Ry (μm)	**6,0**	**5,3**	**6,1**	**4,6**
Standard deviation of Ry	1,6	1,9	2,0	1,3
Average value of Ra (μm)	**1,0**	**1,1**	**1,0**	**1,0**
Standard deviation of Ra	0,2	0,4	0,3	0,3
Average value of Rq (μm)	**1,2**	**1,3**	**1,2**	**1,2**
Standard deviation of Rq	0,2	0,5	0,3	0,4
No. of maps used for statistics	6	4	6	6

3.3 Global roughness via 3D LM

Fig. 10 shows typical LM maps taken on as-obtained cylindrical surfaces of all samples. Despite of the fact that exact determination “what is what” may be tricky, these micrographs make a good image about surfaces.

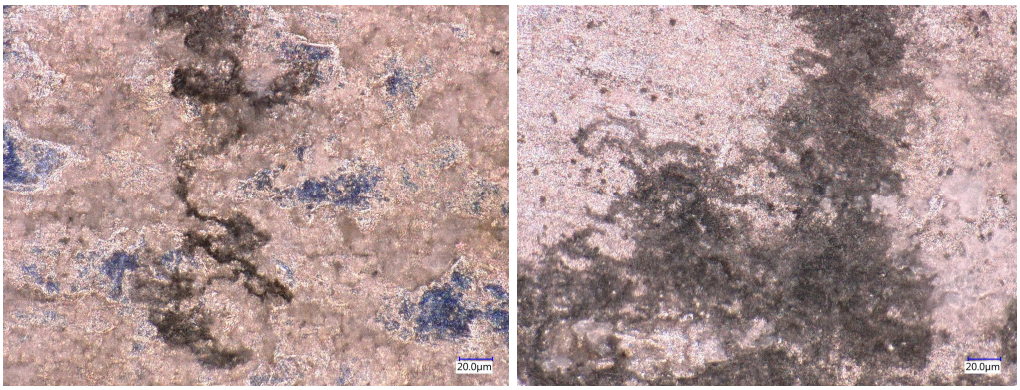

A1 A2

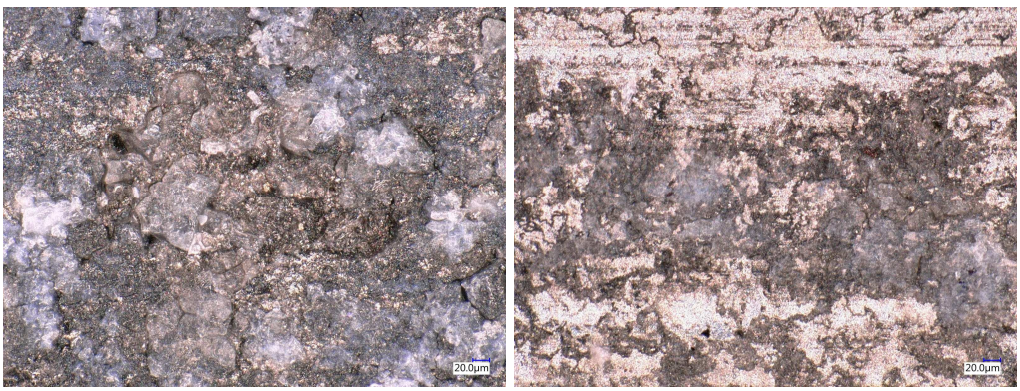

B1 B2

Fig. 10: As-obtained cylindrical surfaces of all samples as viewed by LM at the same magnification (scale bar 20 µm).

In order to describe global surface roughness, 3D LM was employed and obtained data were evaluated via SPIP 6.7.2 software. Only outer surfaces of the samples were measured. Due to cylindrical shapes of the samples and large scale 3D mapping, the surfaces were first recalculated into the plane objects with 2nd order bow correction function implemented in SPIP 6.7.2 software. Typical example of recalculation is shown in Fig. 11.

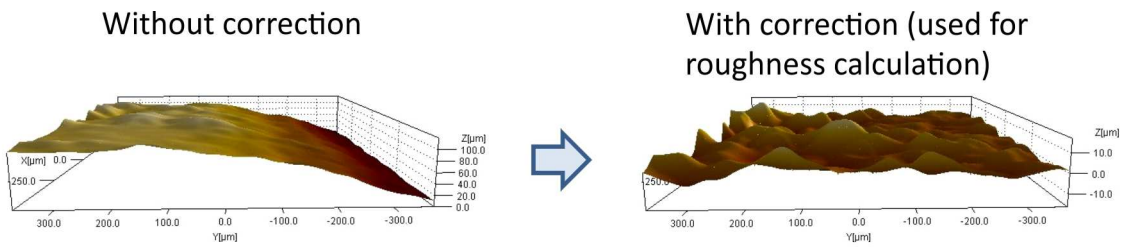

Fig. 11: Typical example of the surface correction due to cylindrical shape of the samples.

Fig. 12 shows examples of 3D LM maps of the surfaces and Tab. 3 lists numerical parameters of the surface roughness extracted from many 3D LM maps. For each sample, we evaluated at least 6 3D LM maps to get reasonable statistics and, thus, reliable results. Despite lower resolution of 3D LM technique in comparison with AFM, the 3D LM results may give more realistic values due to much larger area analysed. The most striking difference between AFM and 3D LM was found for B1 sample (compare Tab. 2 and Tab. 3). Probable reason is rather local character of AFM mapping which cannot consider statistically relevant area of the sample for our AFM setup.

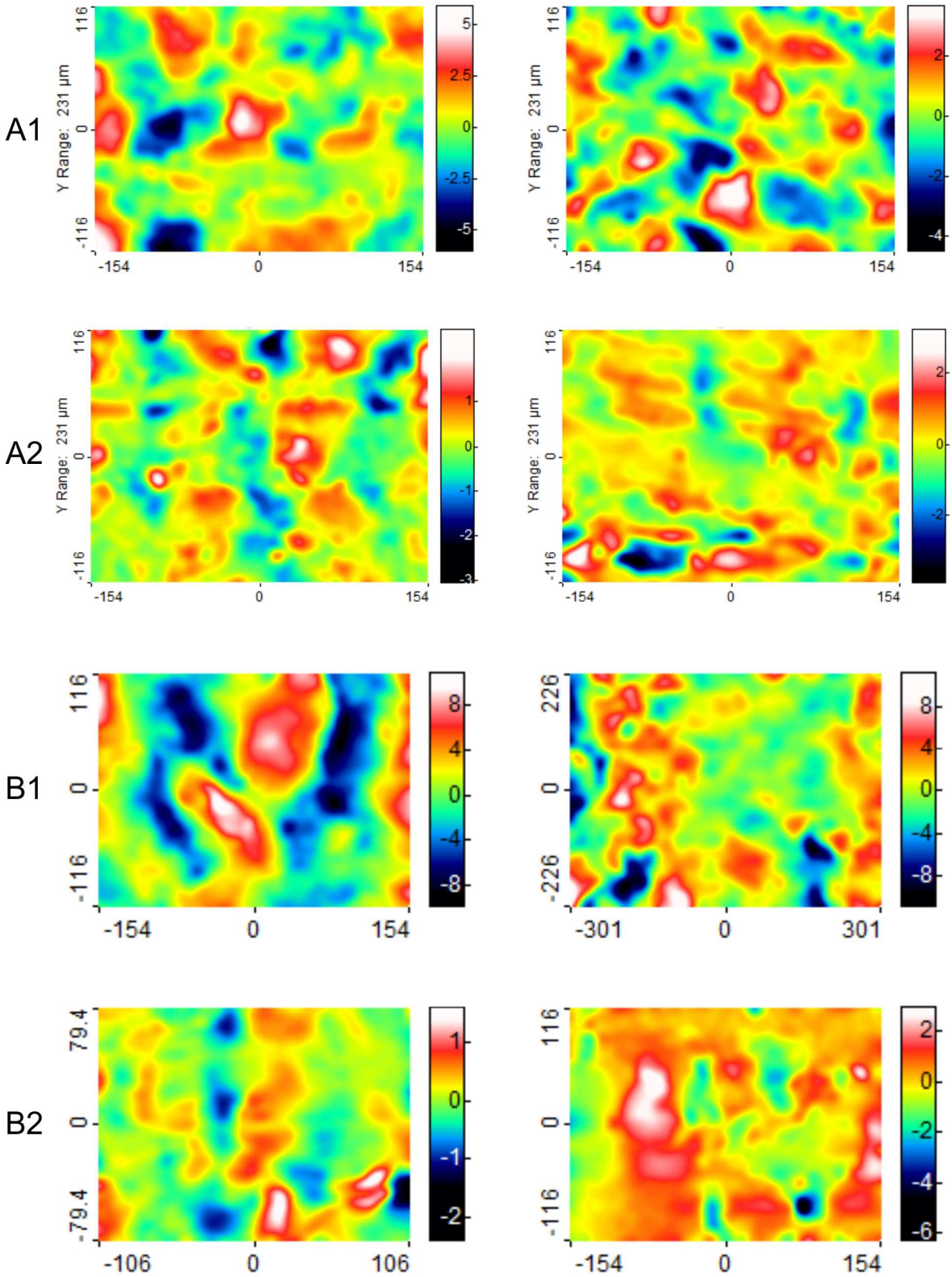

Fig. 12: Typical 3D surfaces of all samples at low magnification (3D LM). Numbers depict dimensions and high profiles in µm.

Tab.3: Global roughnesses Rz (Ten-spot average roughness), Ry (Maximum height), Ra (average roughness) and Rq (root mean square roughness) of the surfaces calculated from 3D light microscopy.

Sample no.	***A1***	***A2***	***B1***	***B2***
Average value of Rz (um)	**9,0**	**6,0**	**25,9**	**8,4**
Standard deviation of Rz	1,2	1,3	10,5	3,7
Average value of Ry (um)	**10,2**	**6,1**	**32,6**	**9,7**
Standard deviation of Ry	1,7	1,2	13,8	4,5
Average value of Ra (um)	**1,0**	**0,5**	**3,6**	**0,8**
Standard deviation of Ra	0,1	0,1	2,5	0,5
Average value of Rq (um)	**1,3**	**0,8**	**4,9**	**1,1**
Standard deviation of Rq	0,2	0,2	3,5	0,7
Area analysed (mm^2)	0,7	1,0	5,2	2,1
No. of maps for statistics	7	6	12	14